Chinese Chemical Letters 34 (2023) 107712

Contents lists available at ScienceDirect

Chinese Chemical Letters

journal homepage: www.elsevier.com/locate/cclet

Electrochemical detection of amino acids based on cucurbit[7]uril-mediated three-dimensional gold nanoassemblies

Shimi Liu[a,1], Hao Zhang[a,1], Yaqi Wang[a], Yan Zeng[a,*], Sobhan Chatterjee[a], Feng Liang[a,b,*]

[a] The State Key Laboratory of Refractories and Metallurgy, School of Chemistry and Chemical Engineering, Wuhan University of Science and Technology, Wuhan 430081, China
[b] Improve-WUST Joint Laboratory of Advanced Technology for Point-of-Care Testing and Precision Medicine, Wuhan University of Science and Technology, Wuhan 430081, China

ARTICLE INFO

Article history:
Received 9 May 2022
Revised 25 July 2022
Accepted 25 July 2022
Available online 29 July 2022

Keywords:
Cucurbit[7]uril
Gold nanoassemblies
Amino acids
Electrochemical detection
Host-guest interactions

ABSTRACT

In this paper, cucurbit[7]uril (CB[7])-mediated three-dimensional gold nanoassemblies were successfully prepared to increase the loaded amount of CB[7] and enhance the electrochemical detection of amino acids. Particle sizes of gold nanoparticles (AuNPs) significantly affect stability and detection sensitivity of nanoassemblies. The volume of gold nanoassemblies first increased and then decreased with the increase of CB[7] concentration. The 3D gold nanoassemblies composed of 16 nm AuNPs and 100 μmol/L CB[7] had excellent stability and maximum volume, exhibiting more sensitive detection for a variety of amino acids. And the detection limits of aromatic amino acids are lower in virtue of the higher binding constant between aromatic amino acids and CB[7]. This study will develop and deepen our understanding of molecular recognition in amino acids detection.

Amino acids, as the main component of proteins, are one of the basic substances for life-sustaining activities and important physical health indicators [1]. The detection of amino acids is extremely valuable for optimizing the dietary structure, maintaining body health, and early diagnosis of disease [2–4]. Therefore, rapid, simple and sensitive detection of amino acids have attracted significant attentions. Many detection methods based on high-performance liquid chromatography-mass spectrometry [5], colorimetry [6], Raman spectroscopy [7], fluorescence [8–10] and electrochemistry [11,12] have been developed in recent years. Among of them, electrochemical impedance spectroscopy (EIS), a non-destructive and non-marking detection method, is suitable for amino acids detection at low concentration because of its high sensitivity and accuracy. To enhance the sensitivity of the electrochemical detection, surface modification of the electrode is a powerful means [13], which could be beneficial for free amino acids to contact the surface of the electrode.

Cucurbit[*n*]urils (CB[*n*]s, $n = 5, 6, 7, 8, 10$) are synthetic macrocyclic host molecules with hydrophilic portals and hydrophobic cavity [14]. And the internal cavity of CB[*n*]s can form complexes with some organic molecules through non-covalent interactions [15–18]. Specifically, CB[*n*]s as the host molecules can recognize various specific amino acids, peptides and proteins in the solution and gas phase [19–21]. For example, CB[6] possesses a strong binding force with the chain amino acids leucine and methionine [22]. Moreover, CB[7] forms stable host-guest complex with most amino acids and is widely used for amino acids detection [19,23]. Thus, CB[7] modified on the surface of the electrode will capture free amino acids in the solution through host-guest interactions and produce an obvious electrochemical signal. On the other hand, CB[*n*]s-mediated noble metal nanoparticles exhibit better stability and optical properties [24], extending their applications in detection. For example, based on the molecular recognition of CB[6] and the surface plasmon resonance effect of silver nanoparticles (AgNPs), He and coworkers used CB[6]-modified AgNPs as a visual probe to detect metformin (MET) [25]. Chen and coworkers prepared an unlabeled impedance sensor by combining CB[7] with gold nanoparticles (AuNPs) to detect amphetamine-type stimulants [26]. Our group prepared a series of CB[*n*]-wrapped AuNPs in alkaline aqueous solution [27], and achieved MET recognition detection with a detection limit of 1.8 pmol/L [28]. We also studied the host-guest interaction of CB[7] with phenyl, adamantyl and ferrocene groups on the gold surface [29], and explored the influence of CB[7] host-guest interaction on ferrocene-modified gold

* Corresponding authors at: The State Key Laboratory of Refractories and Metallurgy, School of Chemistry and Chemical Engineering, Wuhan University of Science and Technology, Wuhan 430081, China
E-mail addresses: zengyan@wust.edu.cn (Y. Zeng), feng_liang@whu.edu.cn (F. Liang).
[1] These authors contributed equally to this work.

https://doi.org/10.1016/j.cclet.2022.07.055
1001-8417/

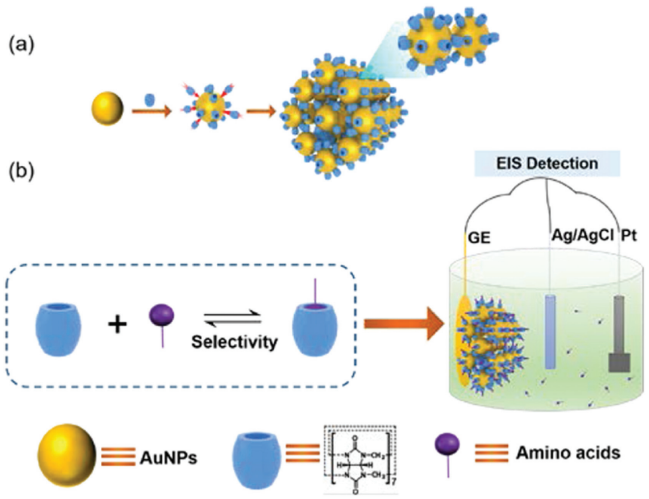

Fig. 1. (a) Schematic representation of 3D-AuNPs@CB[7] formed by the self-assembly of AuNPs and CB[7]. (b) Schematic representation of electrochemical detection of amino acids based on 3D-AuNPs@CB[7].

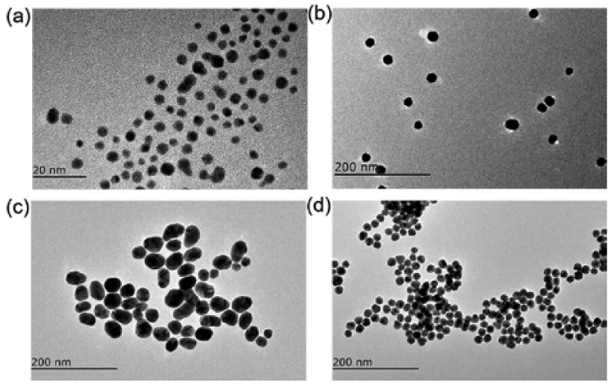

Fig. 2. TEM images of (a) 4 nm AuNPs, (b) 16 nm AuNPs, (c) 40 nm AuNPs and (d) 3D-16 nm AuNPs@CB[7].

nanoelectrode, providing new insights into the interaction process of supramolecular systems [30].

Typically, CB[7] is directly modified on the electrode surface to capture amino acids, but the amount of CB[7] on the electrode surface is limited and the increase of sensitivity and detection range is restricted by the surface area of the electrode [31]. Therefore, increasing the content of CB[7] can improve the detection sensitivity of amino acids based on EIS. Herein, three-dimensional gold nanoassemblies (3D-AuNPs@CB[7]) formed by the self-assembly of AuNPs and CB[7] were successfully prepared for the detection of amino acids (Fig. 1). 3D-AuNPs@CB[7] increased the loaded amount of CB[7], effectively enhancing the detection effect. Interestingly, the detection limits towards aromatic amino acids are lower due to the higher binding constant between aromatic amino acids and CB[7].

The electrochemical performance of AuNPs directly correlated to the particle size of AuNPs [32]. Therefore, AuNPs with different sizes were used for our electrochemical experiments. All AuNPs were prepared at the same initial concentration of $HAuCl_4$ (0.25 mmol/L). The synthesized particle sizes of AuNPs were ~4 nm, 16 nm and 40 nm which were analyzed by UV-vis spectra, dynamic light scattering (Fig. S1 in Supporting information) and transmission electron microscopic (TEM) (Fig. 2).

CB[7] has carbonyl oxygens at both ends, which can be directly connected to the gold surface. The interaction between carbonyl oxygens and the gold surface has prompted CB[7] as a viable strategy for the self-assembly of gold nanoparticles [33]. From Fig. S2 (Supporting information), with the addition of CB[7], AuNPs were assembled and the maximum absorption peaks of AuNPs had a significant redshift, indicating the formation of nanoassemblies. In addition, the maximum absorption peaks of AuNPs first red-shifted and then blue-shifted with the increases of CB[7] concentration [33,34]. And the color of the solution (16 nm AuNPs, Fig. S3 in Supporting information) gradually changed from light pink to light red, to blue-purple, and finally to purple, suggesting that the volume of gold nanoassemblies first increased and then decreased. The volume change of gold nanoassemblies was also observed from dynamic light scattering experiments. As shown in Fig. S4 and Table S1 (Supporting information), the hydraulic radius of AuNPs continuously increased from 25.4 ± 1.3 nm to 1627.4 ± 78.4 nm with the increases in CB[7] concentration from 0 to 100 μmol/L. And the hydraulic radius of AuNPs abruptly reduced to 203.9 ± 11.5 nm when the CB[7] concentration reached 1 mmol/L. This could be attributed to the fact that AuNPs would be saturationally covered by CB[7] at high concentration, and could not make contact with each other and undergo self-assembly. When the redshift of AuNPs reached the maximized value, the gold nanoassemblies had the largest volume when the concentrations of CB[7] is 10 μmol/L (for 4 nm AuNPs), 100 μmol/L (for 16 nm AuNPs), and 10 μmol/L (for 40 nm AuNPs) respectively. These results illustrated that the concentration of CB[7] affected the volume of gold nanoassemblies. In addition, it was found that compared to 4 nm and 16 nm AuNPs, 40 nm AuNPs could produce the biggest particle but with bad stability (Fig. S5 in Supporting information). In general, the larger the size of AuNPs, there is more CB[7] on the surface of each AuNP [29]. We had calculated the load rates of CB[7] on the surface of gold nanoassemblies by thermo-gravimetric analysis (TGA). As shown in Fig. S6 (Supporting information), there were two steps to weight loss. The first step was the release of physically absorbed water up to 300 °C. The second step was the thermal decomposition process of CB[7] above 370 °C [35,36]. The results showed that the load rates of CB[7] on the surface of assemblies composed of 4 nm and 16 nm AuNPs were 4.22% and 8.76% (Fig. S6 in Supporting information). Therefore, the load rate of CB[7] on the surface of 16 nm AuNPs was higher, which is consistent with our previous results [29]. However, the 3D gold nanoassemblies composed of 40 nm AuNPs and CB[7] had worse stability, and the load rate of CB[7] on the surface of gold nanoassemblies could not be precisely measured.

3D structures of gold nanoassemblies were further confirmed by TEM, Energy-dispersive X-ray spectroscopy (EDS) (Figs. S7a and b in Supporting information), and atomic force microscopy (AFM). Compared with well-dispersed AuNPs (16 nm) without CB[7], AuNPs appeared obvious aggregation from the TEM image (Fig. 2d) in presence of CB[7]. The result of elemental analysis showed that N element distributed on the surface of AuNPs, which indicated that CB[7] was successfully assembled on AuNPs (Fig. S7). Moreover, well-dispersed AuNPs (16 nm) and the corresponding gold nanoassemblies were measured by AFM. In the AFM images (Fig. 3), one of the AuNPs (16 nm) without CB[7] was around 10 nm and the corresponding gold nanoassemblies were more than 450 nm, demonstrating the 3D structures formation of gold nanoassemblies.

After obtaining the biggest nanoassemblies, these 3D gold nanoassemblies were simply added dropwise to the gold electrode (GE) and easily modified to the GE surface, due to the interaction between GE and CB[7] on the gold nanoassemblies. As seen from the scanning electron microscopy (SEM, Fig. S8 in Supporting information), large numbers of AuNPs were aggregated together on the GE surface, illustrating that 3D-AuNPs@CB[7] were successfully modified to the GE. EIS Nyquist plots (Fig. 4a) also confirmed successful modification. Due to the high conductivity of AuNPs, 3D-AuNPs@CB[7] composed of AuNPs with different particle sizes all

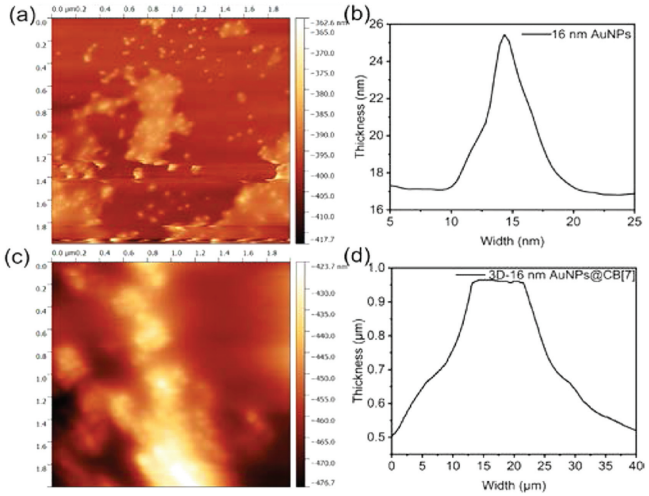

Fig. 3. AFM images of (a) 16 nm AuNPs and (c) the corresponding nanoassemblies (3D-16 nm AuNPs@CB[7]). And height analysis of (b) 16 nm AuNPs and (d) 3D-16 nm AuNPs@CB[7].

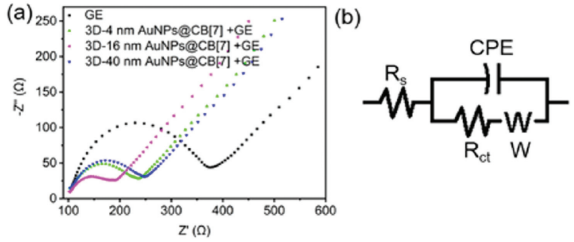

Fig. 4. (a) Nyquist plots for different modified electrodes in the electrolyte solution. (b) The equivalent circuit model was used to fit the Nyquist plots.

enhanced electron transfer and reduced the R_{ct} value. The EIS data is calculated using the equivalent circuit shown in Fig. 4b. The model linearly diffuses the surface of the electrode using the Warburg impedance (W) and R_{ct}. The constant-phase element (CPE) is the double-layer capacitance. R_s and R_{ct} are the solution resistance and charge transfer resistance respectively.

In electrochemical detection, the effect of the AuNPs particle size has been explored. As the increase of L-phenylalanine (L-Phe) concentration, the R_{ct} values of 3D-AuNPs@CB[7] increased (Fig. S9 in Supporting information). Similarly, the linear relationship between the concentrations of L-Phe and the change values of R_{ct} (ΔR_{ct}) suggests that the 3D-AuNPs@CB[7] could affect the detection of L-Phe. Meanwhile, the particle size of AuNPs has an impact on detection range and detection limit with the same concentration of CB[7] modified on 3D-AuNPs@CB[7]. For example, 16 nm and 40 nm AuNPs have lower detection limit than 4 nm AuNPs, indicating that the large particle size of AuNPs has contributed to the detection limit. Furthermore, 40 nm AuNPs have a lower detection range than that of 4 nm and 16 nm AuNPs. The effect of the concentration of CB[7] on gold nanoassemblies was also studied. With the increase of CB[7] concentration , the detection sensitivity has been greatly improved (Fig. S10 in Supporting information). When the concentration of CB[7] was 100 μmol/L, 16 nm AuNPs not only had the maximum redshift and volume but also performed the best detection range, the lowest detection limit and excellent linear relationship. Therefore, 3D-AuNPs@CB[7] composed of 16 nm AuNPs and 100 μmol/L CB[7] were selected in the following electrochemical experiments.

Multiple amino acids were detected by EIS, and 3D-AuNPs@CB[7] showed an excellent detection effect (Fig. S11 in Supporting information). With the increase of concentration,

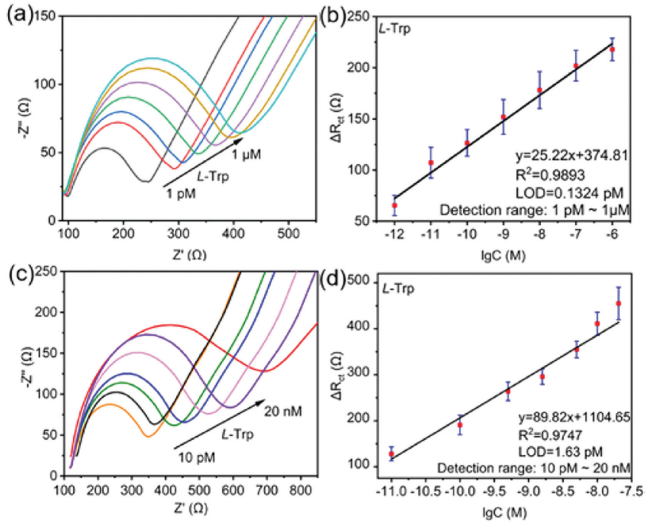

Fig. 5. (a) Nyquist plots for 3D-AuNPs@CB[7] incubated with different concentrations of L-Trp (1 pmol/L, 10 pmol/L, 100 pmol/L, 1 nmol/L, 10 nmol/L, 100 nmol/L, 1 μmol/L). (b) Calibration curves of ΔR_{ct} value *vs.* concentration of L-Trp with 3D-AuNPs@CB[7] modified electrode. (c) Nyquist plots for CB[7] incubated with different concentrations of L-Trp (0.01, 0.1, 0.5, 1.5, 5, 10, 20 nmol/L). (d) Calibration curves of ΔR_{ct} value *vs.* concentration of L-Trp with CB[7] modified electrode.

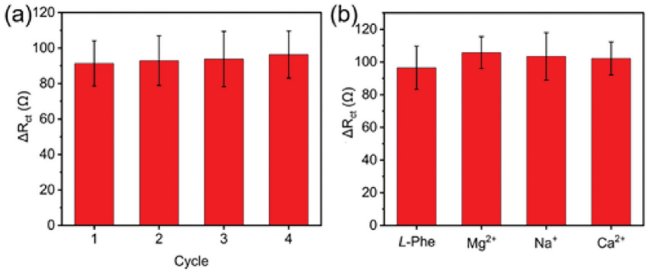

Fig. 6. (a) Cycling test of 3D-AuNPs@CB[7] modified electrode for detection of 1 pmol/L L-Phe. (b) ΔR_{ct} values of 3D-AuNPs@CB[7] modified electrode obtained for L-Phe (1 pmol/L) and different interfering substances added (Mg^{2+}, Na^{+}, Ca^{2+} at a concentration of 0.03 mg/mL). Error bars represent standard deviations of the measurements ($n = 4$).

amino acids have more chance to be adsorbed on the surface of the electrode through host-guest interactions, leading to the hindered electron transfer and sustained growth of R_{ct}. More specifically in this research article uses the modified CB[7] on the surface of GE to conduct control experiments. As shown in Fig. 5, Figs. S11 and S12 (Supporting information), the detection limit of only modified CB[7] electrode surface is higher than that of modified 3D-AuNPs@CB[7], indicating the superior sensing performance of 3D-AuNPs@CB[7]. Similarly, the linear relationship between the concentrations of amino acids and ΔR_{ct} also indicated the sensing performance of 3D-AuNPs@CB[7] towards a variety of amino acids, which is resulted from host-guest interactions.

The host-guest interaction has an important impact on detection. Aromatic amino acids L-Phe and L-tryptophan (L-Trp) have a stronger binding with CB[7] than L-histidine (L-His), L-lysine (L-Lys), and proline (Pro) amino acids [37], indicating that aromatic amino acids would be adsorbed on 3D-AuNPs@CB[7] more easily and the detection limit was lower than L-His, L-Lys and Pro (Table S2 in Supporting information). To evaluate the stability and selectivity of 3D-AuNPs@CB[7], the sensing experiments of 3D-AuNPs@CB[7] towards L-Phe were performed in the absence and presence of potentially interfering substances (Mg^{2+}, Na^{+} and Ca^{2+}) and repeated sensing process up to four times (Fig. 6). The

stable R_{ct} change values illustrated the feasibility and reliability of 3D-AuNPs@CB[7] for the electrochemical detection of amino acids.

In conclusion, CB[7]-mediated three-dimensional gold nanoassemblies were successfully prepared and effectively improved the loaded amount of CB[7]. In the electrochemical experiments, the particle size of AuNPs and the volume of gold nanoassemblies all affected the detection of amino acids. 3D-AuNPs@CB[7] composed of 16 nm AuNPs and 100 μmol/L CB[7] had excellent stability and maximum volume, exhibiting more sensitive detection for a variety of amino acids. The detection limits of aromatic amino acids are lower in virtue of the higher binding constant between aromatic amino acids and CB[7]. Moreover, 3D-AuNPs@CB[7] showed good stability, reproducibility, and anti-interference in electrochemical measurements. The 3D-AuNPs@CB[7] will provide a new research direction for the detection of amino acids.

Declaration of competing interest

The authors declare that they have no known competing financial interests or personal relationships that could have appeared to influence the work reported in this paper.

Acknowledgments

This work was supported in part by grants from the National Natural Science Foundation of China (No. 21871108), the Program for Innovative Teams of Outstanding Young and Middle-Aged Researchers in the Higher Education Institutions of Hubei Province (No. T201702).

Supplementary materials

Supplementary material associated with this article can be found, in the online version, at doi:10.1016/j.cclet.2022.07.055.

References

[1] R.P. Liang, L. Wang, X.Y. Meng, J.W. Wang, J.D. Qiu, Microfluid. Nanofluid. 11 (2011) 227–233.
[2] E.L. Lieu, T. Nguyen, S. Rhyne, J. Kim, Exp. Mol. Med. 52 (2020) 15–30.
[3] M. Onozato, Y. Tanaka, M. Arita, et al., Pract. Lab. Med. 12 (2018) e00099.
[4] X.C. Lin, B. Zhan, S. Wen, et al., Mol. Biosyst. 12 (2016) 2883–2892.
[5] Y. Takagai, K. Yamazoe, T. Sato, et al., J. Chromatogr. A 1621 (2020) 461033.
[6] A. Bahadoran, M.K. Jabarabadi, Z.H. Mahmood, et al., Spectrochim. Acta Part A 268 (2022) 120636.
[7] X.Q. Wang, X.L. Liu, X.T. Wang, et al., Microchim. Acta 189 (2022) 82.
[8] Y.Z. Yang, N. Xiao, S.G. Liu, et al., Mater. Sci. Eng. C 108 (2020) 110401.
[9] N. Tuccitto, L. Fichera, R. Ruffino, et al., ACS Appl. Nano Mater. 4 (2021) 6250–6256.
[10] W.T. Xu, H.M. Feng, W.W. Zhao, et al., Anal. Chim. Acta 1135 (2020) 142–149.
[11] M. Govindasamy, S.F. Wang, W.C. Pan, et al., Ultrason. Sonochem. 56 (2019) 193–199.
[12] E.V. Suprun, E.V. Karpova, S.P. Radko, A.A. Karyakin, Electrochim. Acta 331 (2020) 135289.
[13] H. Zhang, K.T. Huang, L. Ding, et al., Chin. Chem. Lett. 33 (2022) 1537–1540.
[14] H.G. Nie, Z. Wei, X.L. Ni, Y. Liu, Chem. Rev. 122 (2022) 9032–9077.
[15] L.Z. Zhu, Z.Y. Zhao, X.Z. Zhang, et al., Molecules 23 (2018) 947.
[16] S.K. Li, Y. Gao, Y.F. Ding, A.N. Xu, H.P. Tan, Chin. Chem. Lett. 32 (2021) 313–318.
[17] C.H. Kwong, J.F. Mu, S.K. Li, et al., Chin. Chem. Lett. 32 (2021) 3019–3022.
[18] M. Liu, Y. Zhou, L.X. Chen, et al., Chin. Chem. Lett. 32 (2021) 375–379.
[19] E. Kovalenko, M. Vilaseca, D.L. Mireia, et al., J. Am. Soc. Mass Spectrom. 27 (2016) 265–276.
[20] M. Zhang, H. Zhang, L. Jin, et al., Chem. Commun. 58 (2022) 1736–1739.
[21] F. Biedermann, W.M. Nau, Angew. Chem. Int. Ed. 53 (2014) 5694–5699.
[22] C.R. Jiang, Z.R. Song, M. Fizir, et al., Chem. Phys. Lett. 783 (2021) 139039.
[23] K. Bodoor, M.I. El-Barghouthi, K.I. Assaf, et al., J. Incl. Phenom. Macrocycl. Chem. 102 (2022) 159–168.
[24] L.L. Tan, M.Y. Wei, L. Shang, Y.W. Yang, Adv. Funct. Mater. 31 (2021) 2007277.
[25] Z.R. Song, L.L. Yu, Y.Y. Sun, H. He, Anal. Bioanal. Chem. 411 (2019) 7293–7301.
[26] H.J. Li, X.J. Hu, J.L. Zhao, K. Koh, H.X. Chen, Electrochem. Commun. 100 (2019) 126–133.
[27] L.F. Zhang, S.M. Liu, Y.H. Wang, H.J. Zhang, F. Liang, Nanomaterials 8 (2018) 1015.
[28] Y.Q. Wang, L. Ding, H. Yu, F. Liang, Chin. Chem. Lett. 33 (2022) 283–287.
[29] M.Y. Zhang, Z.J. Gong, W.S. Yang, et al., ACS Appl. Nano Mater. 3 (2020) 4283–4291.
[30] Q.S. Ai, L.Q. Jin, Z.J. Gong, F. Liang, ACS Omega 5 (2020) 10581–10585.
[31] Q. An, G.T. Li, C.G. Tao, et al., Chem. Commun. (2008) 1989–1991.
[32] A.J. Wain, Electrochim. Acta 92 (2013) 383–391.
[33] T.C. Lee, O.A. Scherman, Chem. Eur. J. 18 (2012) 1628–1633.
[34] Y.W. Han, X.R. Yang, Y.Z. Liu, et al., Sci. Rep. 6 (2016) 22239.
[35] D. Bardelang, K.A. Udachin, D.M. Leek, et al., Cryst. Growth Des. 11 (2011) 5598–5614.
[36] M. Yoon, K. Suh, H. Kim, et al., Angew. Chem. Int. Ed. 50 (2011) 7870–7873.
[37] J.W. Lee, H.H.L. Lee, Y.H. Ko, K. Kim, H.I. Kim, J. Phys. Chem. B 119 (2015) 4628–4636.